

Electronic Supplementary Information

2-step plasma-enhanced CVD for low-temperature fabrication of silica membranes with high gas-separation performance

5

Toshinori Tsuru,* Hironobu Shigemoto, Masakoto Kanezashi, Tomohisa Yoshioka

10

Department of Chemical Engineering, Hiroshima University, Higashi-Hiroshima 739-8527, Japan ;
E-mail: tsuru@hiroshima-u.ac.jp

15

20 Electronic Supplementary Information-1 (ESI-1):

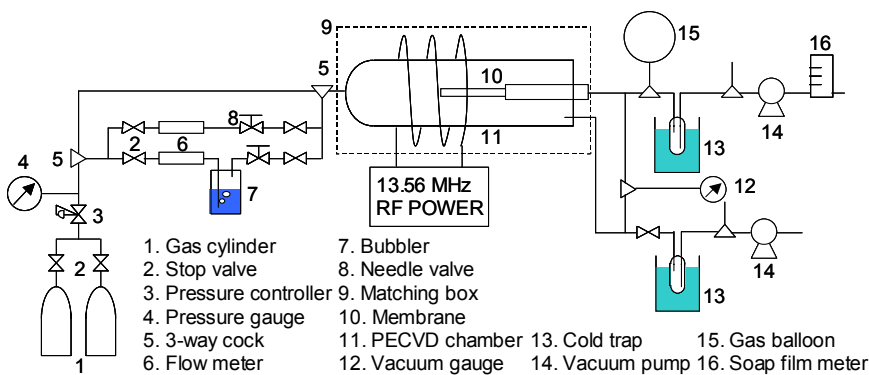
25 Experimental:

1. Plasma CVD

Figure S1 shows the schematic equipment of plasma-enhanced CVD. Ar or O₂ was bubbled through hexamethydisiloxane (HMDSO, Aldrich), which was used without further purification as a Si-source, and fed to a PECVD reactor made of Pyrex glass. RF plasma induced by the coil outside the Pyrex glass reactor was generated at 13.56 MHz. Reactant gases were flowed through the reactor and outgassed after a cold trap. A feed flow rate of Ar or O₂ was fixed at 5 cc/min with a HMDSO mole fraction of 10 mol%, and the pressure of the reaction was maintained at 120 Pa.

30 2. Gas permeation measurement

Gas permeation properties were evaluated using the same apparatus as used in PECVD without removal of the membrane. Gas permeance was evaluated by measuring the pressure increase in the downstream compartment (constant volume: $5.05 \times 10^{-4} \text{ m}^3$) using an MKS Baraton pressure transducer (722A11TBA2FJ). Permeance, Q , was determined from the increase rate (dP_2/dt) of permeate-side pressure, P_2 , with the glass-balloon (volume: v_2). $Q = (dP_2/dt)(v_2/(RT))/A/\Delta P$, where $(dP_2/dt)(v_2/(RT))$ corresponds to the mole flow rate of permeating gas (mol/s), A is the surface area of the membrane (m^2) and ΔP is the pressure difference between the feed and the permeate (Pa).



40 Fig. S1 Schematic PECVD apparatus equipped with gas permeation measurement

3. Preparation of TiO₂/α-Al₂O₃ substrates

Nanoporous $\text{TiO}_2/\alpha\text{-Al}_2\text{O}_3$ substrates were prepared by sol-gel processing. Titaia sols were coated on α -alumina capillary supports (pore size: 150 nm, outer diameter 3 mm, thickness 0.36mm; NOK Corp., Japan) and fired at 500 °C. The details can be found in Ref. 13 (T. Tsuru, K. Ogawa, M. Kanezashi, T. Yoshioka, *Langmuir*, 2010, **26**, 10897).

5

ESI-2:

The pore size distribution of nanoporous titania membranes was evaluated by the nanopermporometry technique (NPP) using a NanoPermPoromete ® (Seika Sangyo, Japan). The basic principle of NPP is based on the capillary condensation of a vapor inside nanopores and its ability to block the permeation of a non-condensable gas, when a mixture of a non-condensable, such as nitrogen, and a condensable vapor, such as hexane and water vapor, is fed into the porous membrane.^{S1} Figure S2 shows that the average pore sizes defined at 50% of dimensionless permeability were approximately 4 nm.

15

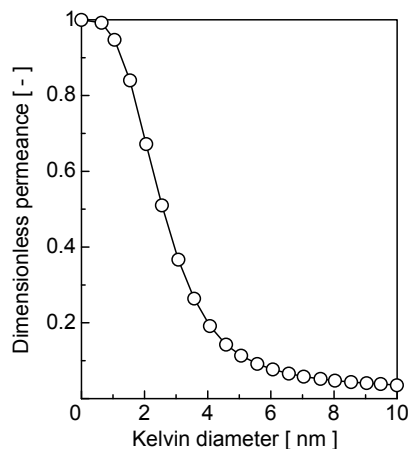


Fig. S2 Pore size distribution of TiO_2 -coated substrate detemined by Nanopermporometry.

20

Reference S1 T. Tsuru, T. Hino, T. Yoshioka, M. Asaeda, *J. Membr. Sci.* **2001**, 186, 257-265.

25

ESI-3:

Cross-sectional SEM of Ar-CVD membranes prepared at different reaction times is shown in Figure S3, and the thickness is plotted as a function of time. The thickness of the Ar-CVD layer increased approximately linearly to the deposition time.

30

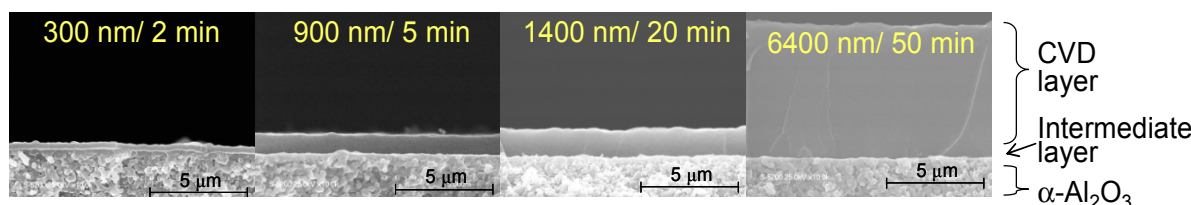


Fig. S3 Cross-sectional SEM of Ar-CVD membranes prepared at different reaction time.

5 ESI-4:

Fig. S5 shows the single gas permeances of He (kinetic diameter: 0.26 nm), N₂ (0.36 nm) and SF₆ (0.55 nm) as a function of the O₂-CVD reaction time. Permeances decreased on the order of 10⁻²-10⁻³ during the initial 20-30 minutes, and then approached steady values. Since the change in permeance was slower than the case in Ar-CVD, thinner and slower film formation was suggested.

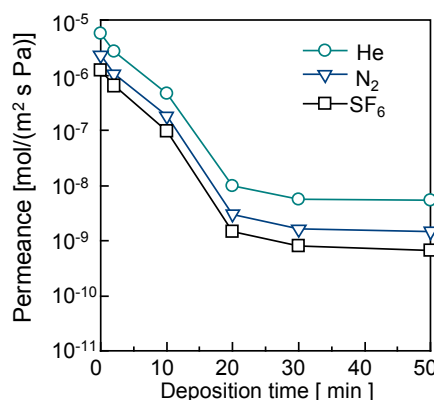


Fig. S4 Single gas permeance of O₂-CVD membrane as a function of CVD reaction time.

10 -----
5 ESI-5:

Cross-sectional SEM of the O₂-CVD membrane (CVD time: 50 min) is shown in Fig. S5. O₂-CVD showed a very different surface morphology from that of Ar-CVD; a large number of silica particle were deposited a much thinner layer was observed.

15

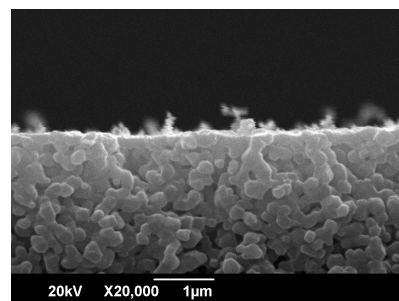


Fig. S5 Cross-sectional SEM of Ar-CVD membranes.

20 -----
5 ESI-6:

It is well accepted that the permeation mechanisms through porous membranes can be categorized as the viscous flow (molecular diffusion), the Knudsen surface diffusion (adsorbed molecules diffuse through porous membranes), and molecular sieving, based on the size ratio of permeating molecules to membrane pores, as well as the interaction between permeating molecules and membrane pore walls.¹⁻³⁾ Among the transport mechanisms, higher CO₂ permeation than He can be explained only by surface diffusion where preferentially adsorbed CO₂ diffuses through an Ar-CVD membrane. CO₂ has been reported to interact with silanol groups in pure SiO₂ membranes,^{2,3)} which may also be the case with Ar-CVD membranes, although we have no experimental data on the affinity of the Ar-CVD layer with CO₂. On the other hand, the 2-step CVD membrane had a dense structure,

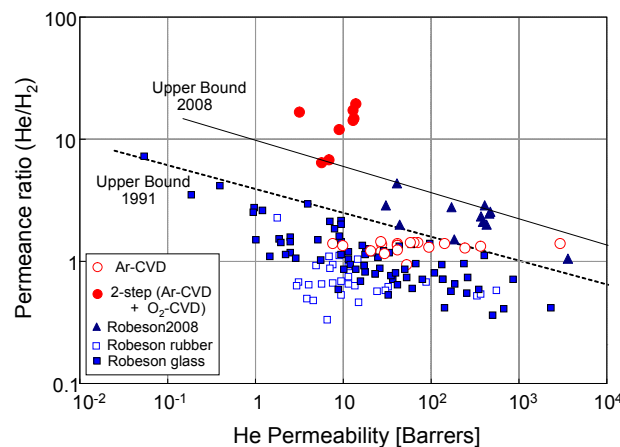
the pore sizes of which became smaller than the size of CO₂, and therefore CO₂ could not permeate through the pores.

- (1) Verweij H, Lin YS, Dong J. Microporous silica and zeolite membranes for hydrogen purification. *MRS Bulletin*, **2006**, 31, 1-10.
5 (2) Shelekhin AB, Dixon AG, Ma YH. Theory of gas diffusion and permeation in inorganic molecular-sieve membranes. *AICHE J.* **1995**, 41, 58-67.
10 (3) Yoshioka T, Nakanishi E, Tsuru T, Asaeda M. Experimental study of gas permeation through microporous silica membranes. *AICHE J.* **2001**, 47, 2052-2063.

10

ESI-7:

- 15 Most polymers showed the separation factor for He/H₂ as approximate unity. Although glassy polymers, especially perfluorinated polymers, showed better performance due to a more rigid structure than rubbery polymers, the maximum permeance ratio was several at maximum.
The permeance ratios of He over H₂ for Ar-CVD membranes were low (approximaltey the same as polymer membranes), while those of 2-step membranes were increased higher than 10. Therefore, it is suggested that
20 through the second step (O₂-CVD), the plasma-polymerized layer formed during Ar-CVD was converted to a silica-rich inorganic layer with high selectivity of He over H₂.



25 Fig. S7 Trade-off curve of separation factor and permeability for the He/H₂ system for polymer membranes (Robeson 1991, 2008) and PECVD membranes.

30

ESI-8:

- Recently, we have found the correlation between the activation energies of H₂ permeation and the permeance ratio of He over H₂. (Reference 9: T. Tsuru, R. Igi, M. Kanezashi, T. Yoshioka, S. Fujisaki, Y. Iwamoto, *AICHE J.*, 2011, **57**, 619.) Figure S8, which summarized approximately all of He/H₂ permeance ratios available in references, shows the correlation of silica membranes, including sol-gel derived membranes, CVD and vitreous glass silica. Surprisingly, irrespective of preparation methods and types of membrane materials, all types of membranes can be expressed with one correlation curve; the permeance ratio of He/H₂ increased with an increase in the activation energy of hydrogen for any type of silica membrane. It should be noted that He/H₂ reported till now was less than 10 at maximum.

40

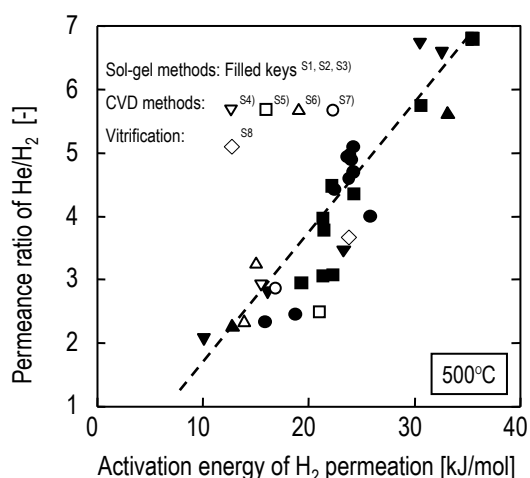


Figure S8. Permeance ratio of He/H₂ as a function of activation energy of hydrogen for various types of silica membranes prepared by sol–gel, CVD, and vitreous silica using different types of materials. (referred from Ref [S1])

5

- [S1] T. Tsuru, R. Igi, M. Kanezashi, T. Yoshioka, S. Fujisaki, Y. Iwamoto, *AICHE J*, 2011, 57, 618.
[S2] Kanezashi M, Asaeda M. Stability of H₂-permselective Ni-doped silica membranes in steam at high temperature. *J. Chem. Eng. Jpn.* **2005**, 38, 908-912.
10 [S3] Mori H, Nagano T, Fujisaki S, Sumino T, Iwamoto Y. Hydrogen permeation through cobalt-doped amorphous silica composite membranes. *Proceedings of 9th International Conference on Inorganic Membranes*, pp. 496-8 (2006)
[S4] Lee D, Zhang L, Oyama ST, Niu S, Saraf, R. F. Synthesis, characterization, and gas permeation properties of a hydrogen permeable silica membrane supported on porous alumina. *J. Membr. Sci.* **2004**, 231, 117-126.
15 [S5] Hacarlioglu P, Lee D, Gibbs GV, Oyama ST. Activation energy for permeation of He and H₂ through silica membranes: An ab initio calculation study. *J. Membr. Sci.* **2008**, 313, 277-283.
[S6] Hwang GH, Onuki K, Shimizu S, Ohya H. Hydrogen separation in H₂-H₂O-HI gaseous mixture using the silica membrane prepared by chemical vapor deposition. *J. Membr. Sci.* 1999, 162, 83-90.
20 [S7] Araki S, Mohri N, Yoshimitsu Y, Miyake Y. Synthesis, characterization and gas permeation properties of a silica membrane prepared by high-pressure chemical vapor deposition. *J. Membr. Sci.* 2007, 290, 138-145.
[S8] Hwang ST., Kammermeyer K. *Membrane in Separation*, John Wiley and Sons, Inc.: 1975

25 -----

ESI-9:

Figure S9 shows a trade-off curve for H₂/N₂ vs. H₂ permeance for amorphous silica membranes. The figure was redrawn from Iwamoto,¹⁾ and membrane performances in recent literature reported later than 2008 have been added to the figure. Permeation properties are categorized with permeation temperatures: 573-473K (square), 473-573K (triangle), and 573-673K (circle). Open keys in the figure and the upper bound line (Upper Bound 2007) are redrawn from Iwamoto,¹⁾ and closed keys are added from references²⁻¹⁴⁾ from 2006-2010. Membrane performances later than 2007 have been improved beyond the upper bound of 2007. The performance of the 2-step PECVD membranes can be plotted close to or beyond the upper-bound line.

35

40

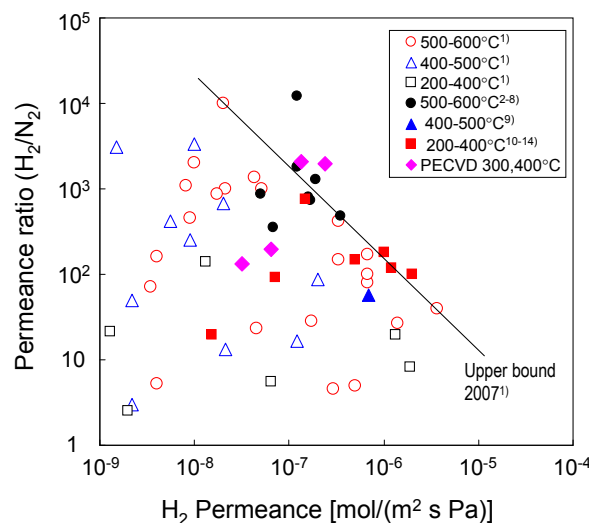


Figure S9. Permeance ratio of H_2/N_2 as a function of H_2 permeance for silica membranes (open keys: redrawn from Iwamoto¹⁾, closed keys: literatures²⁻¹⁴⁾ from 2006-2010)

- 1) Y. Iwamoto, Precursors-derived ceramic membranes for high-temperature separation of hydrogen, *J. Ceram. Soc. Jpn.*, 2007, **115**, 947.
- 2) Mikihiro Nomuraa, Hitoshi Aidaa, Suraj Gopalakrishnana, Takashi Sugawaraa, Shin-ichi Nakaoa, Satoshi Yamazakib, Takeshi Inadab and Yuji Iwamoto, Steam stability of a silica membrane prepared by counterdiffusion chemical vapor deposition, *Desalination*, **193**, 1-7 (2006)
- 3) H. Lim, Y. Gu, S.T. Oyama; "Reaction of primary and secondary products in a membrane reactor: Studies of ethanol steam reforming with a silica–alumina composite membrane," *Journal of Membrane Science*, **351**, p.149-159 (2010)
- 4) T. Nagano, S. Fujisaki, K. Sato, K. Hataya, Y. Iwamoto, M. Nomura, S. Nakao; "Relationship between the Mesoporous Intermediate Layer Structure and the Gas Permeation Property of an Amorphous Silica Membrane Synthesized by Counter Diffusion Chemical Vapor Deposition," *J. Am. Ceram. Soc.*, **91**, p.71–76 (2008)
- 5) Y. Gu, P. Hacarlioglu, S.T. Oyama; "Hydrothermally stable silica–alumina composite membranes for hydrogen separation," *Journal of Membrane Science*, **310** p.28-37 (2008)
- 6) Toshinori Tsuru, Ryousuke Igi, Masakoto Kanezashi, Tomohisa Yoshioka, Shinji Fujisaki, and Yuji Iwamoto, Permeation Properties of Hydrogen and Water Vapor Through Porous Silica Membranes at High Temperatures, *AIChE J.*, **57** (2011)618-629
- 7) Y. Yoshino, T. Suzuki, H. Taguchi, M. Nomura, S. Nakao, N. Itoh; "Development of an All-ceramic Module with Silica Membrane Tubes for High Temperature Hydrogen Separation," *Separation Science and Technology*, **43** p.3432-3447 (2008)
- 8) M. Kanezashi, M. Asaeda; Hydrogen permeation characteristics and stability of Ni-doped silica membranes in steam at high temperature," *Journal of Membrane Science*, p.86-93, **271** (2006)
- 9) S. Gopalakrishnan, J.C.D. da Costa; "Hydrogen gas mixture separation by CVD silica membrane," *Journal of Membrane Science*, **323**, p.144-147 (2008)
- 10) D.E. Koutsonikolas, S.P. Kaldis, S.D. Sklari, G. Pantoleontos, V.T. Zaspalis, G.P. Sakellaropoulos; "Preparation of highly selective silica membranes on defect-free γ -Al₂O₃ membranes using a low temperature CVI technique," *Microporous and Mesoporous Materials*, **132**, p.276-281 (2010)
- 11) D. Koutsonikolas, S. Kaldis, G.P. Sakellaropoulos; "A low-temperature CVI method for pore modification of sol-gel silica membranes," *Journal of Membrane Science*, **342**, p.131-137 (2009)
- 12) Y. Ohta, K. Akamatsua, T. Sugawara, A. Nakao, A. Miyoshi, S. Nakao; "Development of pore size-controlled silica membranes for gas separation by chemical vapor deposition," *Journal of Membrane Science*, **315**, p.93-99 (2008)
- 13) R.M. de Vos, H. Verweij, High-selectivity, high-flux silica membranes for gas separation, *Science*, 1998, **279**, 1710
- 14) M.W.J. Luiten, Nieck E. Benes, Cindy Huiskes, Henk Kruidhof, Arian Nijmeijer, Robust method for micro-porous silica membrane fabrication, *Journal of Membrane Science*, **348**, p.1-5 (2010)

5 ESI-10:

It is commonly accepted that porous membranes such as sol-gel and thermal CVD membranes have pore size distributions. Since gaseous molecules can permeate through pores larger than the molecular sizes, permeances reflect pores larger than the molecular sizes. That is, plus-sieve pore size distribution can be measured by gas molecules of different sizes.

10 The following figure schematically shows the pore size distributions (plus-sieve, normalized with He permeance) of 3 types of porous membranes: M-1, M-2 and M-3. M-1 consisted of a broad pore size distribution ranging from 0.27-0.36 nm, while most pores of M-2 ranged from 0.29 to 0.36. M-3 consisted of a large number of small pores (from 0.27 to 0.29) and a small number of large pores (larger than 0.36nm).

15 The kinetic diameters of He, H₂ and N₂ were 0.26, 0.289, and 0.364nm, respectively. Since permeances are reflected by pore size distribution, the following selectivity can be speculated: M-1 (low He/H₂ selectivity with low He/N₂ selectivity), M-2 (low He/H₂ selectivity with high He/N₂ selectivity), and M-3 (high He/H₂ selectivity with lower He/N₂ selectivity than M-2). M-1, M-2, and M-3 can be categorized to Ar-CVD, 2-step ((Ar-CVD (10 min) + O₂-CVD (5 min)), and 2-step ((Ar-CVD (10 min) + O₂-CVD (30 min), respectively.

20

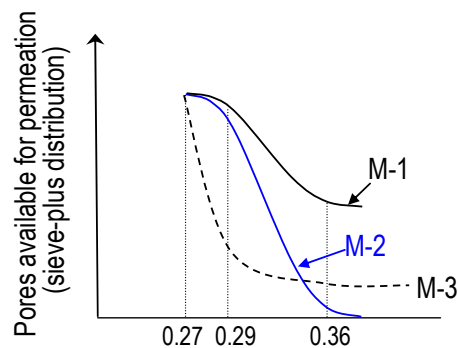


Figure S10. Schematic pore-size distribution of three types of membranes.

25

6 ESI-11

Thermal stability of 2-step PECVD membrane (Ar-CVD (10 min) + O₂-CVD (10 min)) was also examined in the same procedure as in Fig. 4 in the main text. Figure S11 shows the permeances of helium, hydrogen and nitrogen through 2-step PECVD membrane (Ar-CVD (10 min) + O₂-CVD (10 min)). The permeances of helium and hydrogen gradually increased with heat-treatment temperature, while those of N₂ and SF₆ were unchanged or decreased only slightly. Since permeance of N₂ and SF₆, which are relatively large molecules, did not increase, no degradation of the 2-step CVD layer was confirmed. An increase in the permeance of helium and hydrogen can be explained as follows. HMDSO monomer and/or the oligomer, which may have adsorbed to a PECVD layer just after membrane preparation, desorbed or evaporated so as to lead to more space for the permeation of He. Therefore, helium permeance increased and the permeance ratio of He over SF₆ increased from 380 to 4,200, leading to better performance.

40

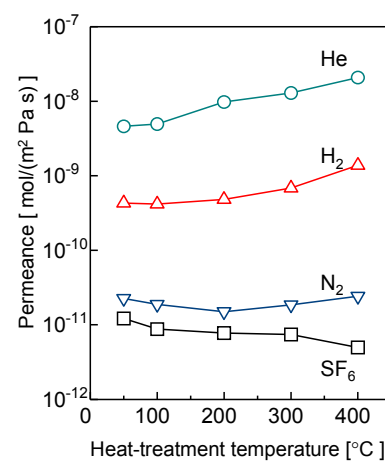


Fig. S11 Single gas permeance at 50°C after heat treatment from 50 to 400°C.